A Molecular Communication Perspective on Airborne Pathogen Transmission and Reception via Droplets Generated by Coughing and Sneezing

Fatih Gulec and Baris Atakan

Abstract—**Infectious diseases spread via pathogens such as viruses and bacteria. Airborne pathogen transmission via droplets is an important mode for infectious diseases. In this paper, the spreading mechanism of infectious diseases by airborne pathogen transmission between two humans is modeled with a molecular communication perspective. An end-to-end system model which considers the pathogen-laden cough/sneeze droplets as the input and the infection state of the human as the output is proposed. This model uses the gravity, initial velocity and buoyancy for the propagation of droplets and a receiver model which considers the central part of the human face as the reception interface is proposed. Furthermore, the probability of infection for an uninfected human is derived by modeling the number of propagating droplets as a random process. The numerical results reveal that exposure time affects the probability of infection. In addition, the social distance for a horizontal cough should be at least 1.7 m and the safe coughing angle of a coughing human to infect less people should be less than $-25°$.**

Index Terms—**Airborne pathogen transmission, molecular communication, probability of infection.**

I. INTRODUCTION

MOLECULAR communication (MC) is an emerging research area which employs chemical signals for information transfer. Originally, MC is proposed as the communication method of the nanomachines mimicking the biological cells in a nanonetwork [1]. MC can also be helpful for practical macroscale applications which include several experimental platforms using molecules or droplets for the information transfer [2]–[7]. Furthermore, MC is utilized to solve practical problems such as finding the distance to a molecular source [8], [9] or the location of this source [10], [11].

Hence, MC can be employed as a tool to model the biological phenomena which consider droplets such as the transmission and reception of pathogens (viruses, bacteria, etc.) which cause contagious diseases via droplets. This concept is first proposed in [12] which consider the infectious human as a blind transmitter (TX) emitting pathogen-laden droplets

and sensors as the receiver (RX) for outdoor environments. This study is improved in [13] by taking silicon nanowire field effect transistor-based biosensors into account to model pathogen detection for airborne pathogen transmission.

Airborne transmission and self-inoculation (direct contact) are two modes of infectious disease transmission via pathogens [14]. Droplets can be classified as large droplets and droplet nuclei (aerosols) which have sizes of larger and smaller than 10 μm, respectively [15]. All expiratory activities such as coughing, sneezing, breathing and speaking can generate large droplets and aerosols. While large droplets can be effective in short-range, aerosols can spread pathogens to longer distances due to their interactions with air. Airborne transmission via droplets is a significant infection mechanism for pathogens such as influenza virus [16], severe acute respiratory syndrome coronavirus-2 (SARS-CoV-2) which causes coronavirus disease 2019 (COVID-19) [17]. It is essential to emphasize that this study is related with the COVID-19 outbreak, since one of the main mechanisms of this disease is airborne transmission.

In fluid dynamics literature for airborne pathogen transmission, the movement of droplets are modeled by considering the gravity, interaction of droplets with air, evaporation, airflows and droplet size [17]. For coughing, [18] proposes a two-stage jet flow model, which is based on experimental data. In [14], the propagation of human sneeze and cough is modeled as a cloud consisting of droplets and air and justified by experimental data for a sneezing/coughing human. Analytical approaches are proposed in [19], [20] to estimate the trajectories of large droplets and aerosols by considering evaporation and turbulent flows for coughing. In [21], a Lagrangian particle model and a discrete random walk model are proposed for the movement of expiratory droplets and turbulent airflows, respectively.

The data collected for airborne pathogen transmission are based on physical experimental setups. These setups consist of humans, thermal manikins or respiratory machines for the emission of droplets, and air samplers or imaging devices to measure droplet concentration after emission [15]. Despite the reliability of collected data from physical setups, computational fluid dynamics (CFD) simulators are preferred more due to their low cost and high resolution in time and space. In CFD simulations, 3-D Navier-Stokes equations are employed with boundary conditions and solved by numerical methods. In [22], the breakup process of droplets, droplet-air interaction and resulting turbulent flows are considered for the movement

of droplets which are emitted by coughing and sneezing with and without a mask. The study in [23] takes into account the effect of evaporation and wind for the dispersion of droplets. [24] proposes a CFD method to model the dispersion of droplets for sneezing and validates it with experimental data.

The aforementioned studies for airborne pathogen transmission focus on the dispersion of droplets for coughing/sneezing. Very few studies such as [25] model the reception of droplets via considering the inhalation rate of a human. In this paper, we investigate airborne pathogen transmission and reception mechanisms between humans with a MC perspective for indoor environments. The infectious human which emit a cloud consisting of pathogen-laden droplets and air by coughing/sneezing is considered as the TX and the uninfected human is defined as the RX unlike the studies in [12], [13] where the RX is a biosensor. Furthermore, the effects of gravity, buoyancy, and air-droplet interactions are taken into account for the indoor propagation of the cloud, which are not considered in [13]. The propagation of the cloud in the MC channel is modeled by modifying the deterministic model in [14] in a probabilistic way. The cloud travels under the influence of initial velocity, buoyancy and gravity. The number of droplets in this cloud is modeled as a random process. A receiver model which takes the central part of human face as the interface with pathogens into account is proposed. The propagation and reception models are employed for the proposed end-to-end system model in order to give the infection state of the RX as the system output. The MC perspective gives the opportunity to handle the airborne pathogen transmission modeling as a system comprising a TX, channel and a RX. Moreover, this perspective enables to approach the estimation of a human's infection state as a binary detection problem according to a threshold defined as the sufficient number of pathogen-laden droplets for infection. The contributions of this paper can be summarized as follows:

- In order to model the spread of the infectious diseases between humans, MC perspective leading us to use and adapt the well-known communication engineering techniques is proposed.
- An end-to-end system model which combines a channel model involving the propagation of pathogen-laden droplets as a cloud and a RX model including the interaction of these droplets with the uninfected human is proposed.
- A probabilistic approach which enables the derivation of the probability of infection for an uninfected human is employed.

Furthermore, the proposed model is evaluated by numerical results. Our key findings for a coughing TX is given as follows:

- Increased exposure time to pathogens increases the probability of infection.
- For a horizontal cough, the social distance should be at least 1.7 m.
- It is safer to cough with an initial angle less than $-25°$ to infect less people.

The rest of the paper is organized as follows. In Section II, the proposed end-to-end system model is presented. Section III
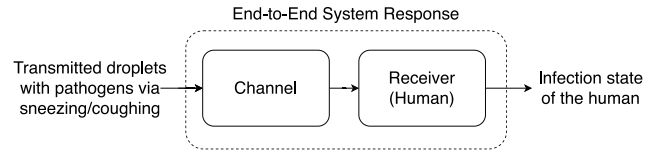

Fig. 1. Block diagram of the end-to-end system model.

provides the derivation of the probability of infection. Numerical results are given in Section IV and the paper is concluded in Section V.

II. END-TO-END SYSTEM MODEL

This section provides a detailed explanation of the proposed end-to-end system model for droplet-based MC between two humans via sneezing/coughing. Here, a sneeze/cough can be considered as an impulsive input signal. Hence, the end-to-end system impulse response is defined as the system's output, which is the infection state, to a sneeze/cough as shown in Fig. 1. Transmitted droplets are modeled as a cloud which is a mixture of air and droplets. As the first step of the end-to-end system model, the trajectory of the cloud is derived. In this study, the model given in [14] for the propagation of the cloud is adopted and modified. In the second step, we derive an end-to-end system model with a probabilistic approach instead of the deterministic approach in [14]. The third step details the RX model which includes signal reconstruction, integration, quantization and detection parts. In the last step, the algorithm for the implementation of the system model is given.

A. Trajectory of the Transmitted Cloud

In our scenario, the TX emits the cloud with an initial velocity on the x-axis by sneezing or coughing. It is assumed that the emitted cloud propagates in still air, i.e., with no ventilation or wind. Due to the warmer air in the mouth (with density ρ_f at $34°C$) with respect to ambient air (with density ρ_a at $23°C$), where $\rho_f < \rho_a$ [26], the emitted cloud is subject to buoyancy on y-axis. As illustrated in Fig. 2, buoyancy, gravity and initial velocity of the cloud affect the trajectory of the cloud. Therefore, the trajectory is defined with the curvilinear s-axis and θ which shows the angle between the s and x axes. During the propagation of the cloud, some of the droplets settle to the ground depending on the gravity and air-droplet interaction. Turbulent flows which are effective at the initial phase of the propagation due to high cloud velocity are not considered. In order to find the position of the cloud in 3-D space, it is essential to derive the time-dependent density of the cloud ($\rho_c(t)$). At the initial state ($t = 0$), the initial cloud mass ($m_c(0)$) can be represented by the addition of the initial droplet mass ($m_d(0)$) and initial air mass in the cloud ($m_a(0)$) as given by [27]

$$m_c(0) = m_d(0) + m_a(0) \tag{1a}$$

$$\rho_c(0)\,V(0) = \rho_d\,V_d(0) + \rho_f(\,V(0) - V_d(0)). \tag{1b}$$

where $V(t)$ is the cloud volume, ρ_d is the droplet density, ρ_f is the air density in the mouth. The volume of droplets in the
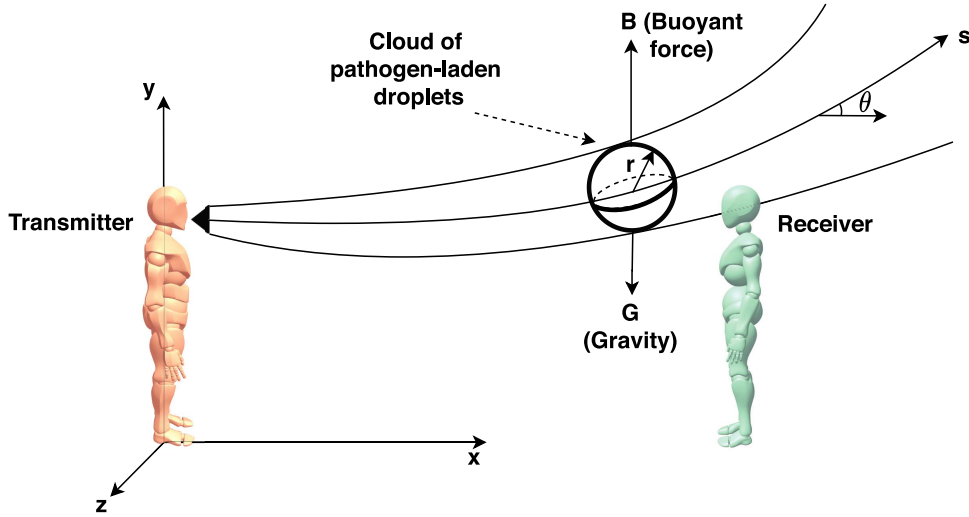
Fig. 2. Trajectory of the cloud between the TX and RX.

cloud ($V_d(t)$) consists of different sized droplets with diameter d_k and can be defined in terms of the volume fraction of droplets ($\phi_k(t)$) in the cloud as $V_d(0) = \sum_{k=1}^{K} \phi_k(0) V(0)$. Here, K is the number of the different droplet sizes, $\phi_k(0) = N_k(0) V_k / V(0)$, $N_k(t)$ and V_k is the number and volume of the spherical droplets of diameter d_k, respectively. $N_k(t)$ changes due to the settling of droplets to the ground as explained in Section II-B. By substituting $V_d(0)$ into (1b) and solving for $\rho_c(0)$, the initial density of the cloud is derived as

$$\rho_c(0) = \sum_{k=1}^{K} (\rho_d - \rho_f)\phi_k(0) + \rho_f. \quad (2)$$

As the cloud moves, it entrains the ambient air with density ρ_a and its volume becomes $V(t) = V(0) + V_a(t)$ where $V_a(t)$ is the acquired air volume. Since the initial volume fraction of the air in the mouth with density ρ_f is relatively small in the moving cloud (10^{-5}) [26], it is assumed as $V(t) \approx V_a(t)$. After the emission of droplets, $\rho_c(t)$ can be derived via the conservation of mass [27]. Hence, the mass of droplets at the time instance t ($m_d(t)$) is equal to the initial mass of droplets ($m_d(0)$) and droplet mass can be expressed by the difference of cloud mass and air mass according to (1a) as given by

$$m_d(t) = m_d(0) \quad (3a)$$

$$\begin{pmatrix} \text{Cloud} \\ \text{mass at } t \end{pmatrix} - \begin{pmatrix} \text{Air} \\ \text{mass at } t \end{pmatrix} = \begin{pmatrix} \text{Initial} \\ \text{cloud mass} \end{pmatrix} - \begin{pmatrix} \text{Initial} \\ \text{air mass} \end{pmatrix} \quad (3b)$$

$$\rho_c(t) V(t) - \rho_a V(t) = \rho_c(0) V(0) - \rho_f V(0). \quad (3c)$$

Via the substitution of (2) into (3c) and some algebraic manipulation, the cloud density is derived as

$$\rho_c(t) = \sum_{k=1}^{K} (\rho_d - \rho_f)\phi_k(t) + \rho_a. \quad (4)$$

As illustrated in Fig. 2, there are two acting forces on the cloud which stem from the gravity and buoyancy on y-axis. Since $\rho_f < \rho_a$, the buoyant force ($B(t)$) affects the movement of the cloud upwards. The net buoyant force acting on the cloud ($F_B(t)$) on y-axis is given by the difference of $B(t)$ and the gravitational force ($G(t)$) as given by [27]

$$F_B(t) = B(t) - G(t) = V(t)\rho_a g - V(t)\rho_c(t)g \quad (5a)$$
$$= V(t)(\rho_a - \rho_c(t))g \quad (5b)$$

where g is the gravitational acceleration.

The movement of the cloud is driven by the momentum (I) which is defined as the multiplication of the mass and velocity [27]. Since it is assumed that there is not any acting force on the cloud for z-axis, I is defined on s-axis and is decomposed into two components on x ($I_x = I \cos(\theta)$) and y axes ($I_y = I \sin(\theta)$). As the cloud moves, its mass increases due to the entrained air and the velocity of the cloud decreases. Since the force can be represented as the derivative of the momentum [27] and there is not any acting force on the x-axis during the propagation, the net force (F_x) on x-axis is given by

$$F_x = \frac{dI_x}{dt} = \frac{dI \cos(\theta)}{dt} = 0. \quad (7)$$

Furthermore, the net force on y-axis, i.e., $F_B(t)$ is given by

$$F_B(t) = \frac{dI_y}{dt} = \frac{dI \sin(\theta)}{dt}. \quad (8)$$

Since the initial buoyancy is conserved as introduced in [14], we have $F_B(t) = F_0$ where F_0 is the net initial buoyant force. With the initial conditions which are $I(0) = I_0$, $\theta(0) = \theta_0$, $I_x(0) = I_0 \cos(\theta_0)$ and $I_y(0) = I_0 \sin(\theta_0)$, I_x and I_y can be given as the solutions of (7) and (8) (considering $F_B(t) = F_0$) as

$$I_x = I_0 \cos(\theta_0), I_y = F_0 t + I_0 \sin(\theta_0). \quad (9)$$

Since there is not any acting force on z-axis, the momentum can be expressed as $I = \sqrt{I_x^2 + I_y^2}$. Due to its definition, the momentum can be written as [27]

$$I = m_c v_c(t) = \rho_c(t) V(t) v_c(t), \quad (10)$$

where we can express the cloud velocity ($v_c(t)$) as the displacement on s-axis ($s(t)$) in an infinitesimal time interval,

i.e., $v_c(t) = ds(t)/dt$. The cloud volume is defined as $V(t) = \eta r(t)^3$ where $\eta = 4\pi/3$ for a spherical cloud. Furthermore, the radius of the cloud ($r(t)$) is linearly related with the distance such that $r(t) = \alpha_e s(t)$ where α_e is the entrainment coefficient and is empirically determined [28]. Hence, (10) can be rewritten as

$$I = \rho_c(t)\eta\alpha_e^3 s(t)^3 \frac{ds(t)}{dt}. \tag{11}$$

When $I = \sqrt{I_x^2 + I_y^2}$ is incorporated into (11), we have

$$\frac{ds(t)}{dt} = \frac{\sqrt{I_x^2 + I_y^2}}{\rho_c(t)\eta\alpha_e^3 s(t)^3}. \tag{12}$$

Here, (4) and (9) are substituted into (12) as given by

$$\frac{ds(t)}{dt} = \frac{\sqrt{F_0^2 t^2 + 2F_0 I_0 sin(\theta_0)t + I_0^2}}{\left(\sum_{k=1}^{K}(\rho_d - \rho_f)\phi_k(t) + \rho_a\right)\eta\alpha_e^3 s(t)^3}. \tag{13}$$

Remembering that $V(t) = \eta\alpha_e^3 s(t)^3$ and $\phi_k(t) = \frac{N_k(t)V_k}{V(t)}$, the denominator part of (13) is simplified as

$$\frac{ds}{dt} = \frac{\sqrt{F_0^2 t^2 + 2F_0 I_0 sin(\theta_0)t + I_0^2}}{Z + \rho_a\eta\alpha_e^3 s^3}, \tag{14}$$

where $Z = \sum_{k=1}^{K}(\rho_d - \rho_f)V_k N_k(t)$.

For convenience, θ_0 is chosen as 0 in [14]. However, $\theta_0 \neq 0$ is also considered in order to observe the effect of the initial cough/sneeze angle in our study. In addition to this, the initial conditions which are $s(0) = 0$ and $t(0) = 0$ are taken into account in the integration of (14) to obtain the quartic equation as given by (6), shown at the bottom of the page. Since the discriminant of the quartic equation (6) is less than zero for physically meaningful parameter values, two of the roots are complex and one of the roots is a real and negative number. Therefore, there is only one possible positive real root which is used as the solution. However, this solution is a very long expression to write in this paper.

In order to determine the trajectory of the cloud, θ needs to be derived. Via the substitution of $I_x = I \cos(\theta)$ and $I_y = I \sin(\theta)$ into (9), two expressions are obtained. Then, by solving these two expressions for I and equating them gives the equation below

$$I = \frac{I_0 \cos(\theta_0)}{\cos(\theta)} = \frac{F_0 t + I_0 \sin(\theta_0)}{\sin(\theta)}. \tag{15}$$

which can be solved for θ as given by

$$\theta = \tan^{-1}\left(\frac{F_0 t}{I_0 \cos(\theta_0)} + \tan(\theta_0)\right). \tag{16}$$

B. Number of Propagating Droplets in the Cloud

After the emission of droplets, some of the droplets settle to the ground due to gravity and their interaction with the air [8], [29]. Therefore, the number of droplets decreases during the propagation due to the settling of droplets. Moreover, it is assumed that the droplets are homogeneously distributed within the cloud and the settling droplets move out of the cloud instantaneously. In addition, since the movement of each droplet in the cloud is assumed to be independent of each other at each time instance, the number of droplets in the cloud can be modeled as a Poisson process with an intensity function $\lambda(t)$ [30]. Here, $\lambda(t)$ which is the mean number of droplets in the cloud can be derived by using the flow rate of the droplets [14]. The flow rate of the droplets (J), which is the derivative of the number of droplets and gives the number of droplets flowing through a surface in unit time (number of droplets/s), is defined as [27]

$$J = \frac{d\lambda(t)}{dt} = vA\bar{\rho}_c(t) \tag{17}$$

where $\bar{\rho}_c(t) = \lambda(t)/V(t)$ and A is the cross-sectional area that droplets are flowing through and v is the velocity of droplets. Since droplets settle through the lower half of the cloud due to the observations in [14], A in (17) is substituted with $A(t)/2$ where $A(t)$ is the surface area of the cloud. Hence, (17) becomes

$$\frac{d\lambda(t)}{dt} = -v_s\frac{A(t)}{2}\frac{\lambda(t)}{V(t)}, \tag{18}$$

where v_s is the settling velocity of droplets and ($-$) sign represents the decrease in the number of droplets due to the settling. For a spherical cloud, when the substitutions $A(t) = 4\pi r(t)^2$, $V(t) = 4\pi r(t)^3/3$ and $r(t) = \alpha_e s(t)$ are made into (18), the rate of change of the mean number of droplets in the cloud is given by

$$\frac{d\lambda(t)}{dt} = \frac{-3v_s\lambda(t)}{2r(t)} = \frac{-3v_s\lambda(t)}{2\alpha_e s(t)}. \tag{19}$$

Since the solution of (6) is very long and makes the solution of (19) very complicated, the trajectory and number of droplets can be found numerically for each time instance. Furthermore, the number of droplets can be different for each droplet size. Thus, (19) is manipulated to derive the change of the mean number of droplets at each time instance ($\Delta\lambda$) as given by

$$\Delta\lambda = \frac{-3v_{s_{k,i}}\lambda_{k,i}\Delta t}{2\alpha s_{k,i}}, \tag{20}$$

where Δt is the time step, the subscripts i and k show the corresponding variables at $t = t_i$ for the droplets of diameter d_k. At each time step, t_i is increased by Δt and the mean

$$\frac{\eta\alpha^3\rho_a}{4}s(t)^4 + Zs(t) - \left(\frac{F_0 t + I_0 sin(\theta_0)}{2F_0}\right)\sqrt{F_0^2 t^2 + 2F_0 I_0 sin(\theta_0)t + I_0^2}$$
$$- \left(\frac{I_0^2\left(sin(\theta_0)^2 - 1\right)}{2F_0}\right)\ln\left(2F_0\sqrt{F_0^2 t^2 + 2F_0 I_0 sin(\theta_0)t + I_0^2} + 2F_0^2 t + 2F_0 I_0 sin(\theta_0)\right) = 0 \tag{6}$$

number of droplets of diameter d_k in the cloud is increased via $\lambda_{k,i+1} = \lambda_{k,i} + \Delta\lambda$. For each time step and droplet size, the number of droplets in the cloud ($N_{k,i}$) follows a Poisson distribution with the rate $\lambda_{k,i}$ [30]. Due to the large number of emitted droplets, this Poisson distribution can be approximated as a Gaussian distribution with a mean and variance $\lambda_{k,i}$ [31]. Hence, $N_{k,i}$ is represented as $N_{k,i} \sim \mathcal{N}(\lambda_{k,i}, \lambda_{k,i})$.

Settling velocities of droplets during the propagation are defined according to the flow regimes which are Newton's (turbulent) flow, intermediate flow and Stokes (laminar) flow regimes [32]. These regimes are determined according to Reynolds number (Re) which is a dimensionless coefficient showing the flow type of the fluid as defined by [27]

$$Re_{k,i} = \frac{d_{k,i}\rho_a v_{c_{k,i}}}{\mu_a}. \tag{21}$$

Equation (21) shows that $Re_{k,i}$ depends on the changing cloud velocity and droplet diameter at each time step. The settling velocities according to the aforementioned flow regimes are derived in the Appendix. The result of these derivations are given by [32]

$$v_{s_{k,i}} = \begin{cases} \dfrac{gd_{k,i}^2(\rho_d - \rho_a)}{18\mu_a}, & Re < 2 \quad\quad (22a) \\ & \text{(Stokes flow)} \\ \dfrac{gd_{k,i}^{8/5}(\rho_d - \rho_a)}{13.875\rho_d^{2/5}\mu_a^{3/5}}, & 2 \le Re \le 500 \quad (22b) \\ & \text{(Intermediate flow)} \\ \dfrac{3.03gd_{k,i}(\rho_d - \rho_a)}{\rho_d}, & 500 < Re \le 2 \times 10^5. \\ & \text{(Newton's flow)} \quad (22c) \end{cases}$$

The effective factors for the cloud are gravity, buoyancy, and different flow regimes generated due to the initial velocity and different droplet sizes as given above. In Newton's and intermediate flow regime, the trajectory of the cloud is dominated by their high horizontal velocity with respect to gravity and buoyancy. However, in Stokes flow, the buoyancy and gravity is much more effective, since droplets lose most of their initial momentum in the horizontal axis. The effect of the turbulent flows is only considered to calculate the settling velocities of the droplets, not for the velocity distribution of them.

C. Receiver Model

Airborne pathogen transmission via droplets is infectious, since emitted pathogen-laden droplets can be sensed by nose, mouth and eyes [15], [33]. Hence, the human face is where the sensing of the infectious pathogens mostly occurs. Even if the pathogens are not directly received via the facial sensory organs, it is possible to become infected by directly touching the face and sensory organs consecutively. With this motivation, the cross-sectional area of the central part of the human face is considered as the RX cross-section as shown in Fig. 3. Moreover, a receiver model is proposed for the reception of droplets as shown in Fig. 4.

As the first step of the reception, the droplets in the vicinity of the RX is sensed by the human, which is defined
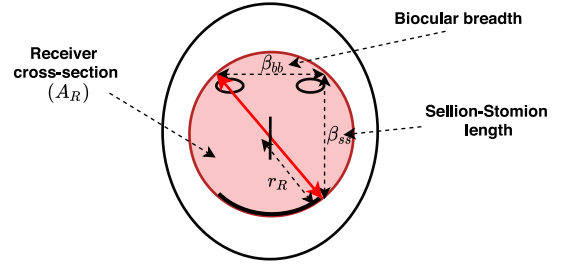

Fig. 3. Receiver cross-section in the human face.

as the signal reconstruction. Different signal reconstruction models for a sensor in macroscale and a nanomachine in microscale are proposed in [3] and [34], respectively. As given in Fig. 3, the RX is assumed to be the cross-section of the human face. In order to determine a circular cross-section area (A_R) for the RX by encompassing the eyes, mouth and nose, a right-angled triangle whose sides are biocular (biectocanthus) breadth (β_{bb}), Sellion-Stomion length (β_{ss}) and the diameter of the receiver cross-section ($2r_R$) as the hypotenuse side is formed as depicted in Fig. 3. Here, β_{bb} is the length of the line connecting the outer end points of the left and right eyes (eyelid junctions) and β_{ss} is the vertical distance between the eye and mouth [35]. Hence, the radius of the cross-sectional area of the RX (r_R) is given as $r_R = (\sqrt{\beta_{bb}^2 + \beta_{ss}^2})/2$.

When the cloud is transmitted via sneezing/coughing, there are three cases for the interaction of the RX and the cloud of droplets with diameter d_k whose centers are at the positions for the ith time step (x_R, y_R, z_R) and ($x_{k,i}, y_{k,i}, z_{k,i}$), respectively. The relation between the 3-D Cartesian coordinates and curvilinear s-axis is detailed in the next subsection. In the first case, the cloud and RX do not coincide and there is no reception. The other two cases include the reception of droplets. As illustrated in Fig. 5, when the cloud and RX coincide, the reception of droplets is related with the cross-sectional area of the cloud at $x_{k,i} = x_R$ ($A_{CS_{k,i}}$), A_R and their intersection area ($A_{RC_{k,i}}$). The second case occurs when the intersection area is less than or equal to the cross-sectional area of the RX, i.e., $A_{RC_{k,i}} < A_R$. In the last case, the cloud encompasses the RX, i.e., $A_{CS_{k,i}} \ge A_R = A_{RC_{k,i}}$.

For the case shown in Fig. 5, $A_{RC_{k,i}}$ can be derived by calculating the intersection area of two circles as given by (23), shown at the bottom the next page, [36] where the distance between the centers of $A_{RC_{k,i}}$ and A_R ($d_{RC_{k,i}}$) is defined as given below.

$$d_{RC_{k,i}} = \sqrt{\left(y_R - y_{k,i}\right)^2 + \left(z_R - z_{k,i}\right)^2}. \tag{24}$$

The received number of droplets can be derived by multiplying the time step (Δt) with the flow rate of the droplets (J in number of droplets/s) at each time step. Since the RX senses the droplets proportional to $A_{RC_{k,i}}$, the received signal after the signal reconstruction step for the aforementioned
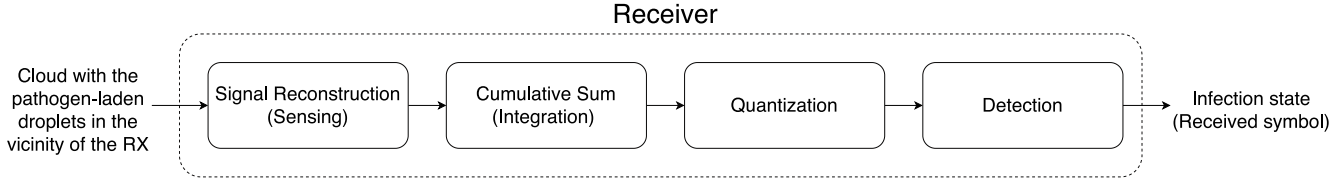
Receiver

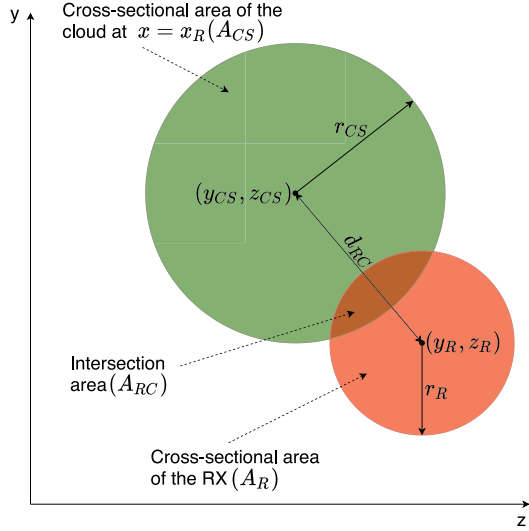Fig. 4.   Block diagram of the receiver model.

Fig. 5.   Intersection of the RX and the cloud cross-section.

cases at each time step by recalling (17) is expressed as

$$\tilde{N}_{R_i} = \begin{cases} \sum_{k=1}^{K} v_{c_{k,i}} A_{RC_{k,i}} \dfrac{N_{k,i}}{\eta r_{k,i}^3} \Delta t, & A_{RC_{k,i}} < A_R \quad (25a) \\[2ex] \sum_{k=1}^{K} v_{c_{k,i}} A_R \dfrac{N_{k,i}}{\eta r_{k,i}^3} \Delta t, & A_{RC_{k,i}} = A_R \quad (25b) \\[2ex] 0, & \text{otherwise}, \quad (25c) \end{cases}$$

where $A_{RC_{k,i}} = \pi r_{RC_{k,i}}^2$, $A_R = \pi r_R^2$, $\eta = 4\pi/3$ and the volume is $\eta r_{k,i}^3$ for the spherical cloud.

As the time elapses, the cumulative exposure to the pathogen-laden droplets at the RX can be modeled by the cumulative sum (integration) of droplets with respect to time subsequent to the signal reconstruction step as given in Fig. 4. Afterwards, the signal is quantized, since the rate of the change in the mean number of droplets may not be an integer. The number of droplets after the cumulative sum is rounded to the nearest integer in the quantization step. The received signal

after the quantization step is given by

$$N_{R_i} = \begin{cases} \sum_{k=1}^{K} \bar{N}_{R_{k,i}}, & A_{RC_{k,i}} < A_R \quad (26a) \\[2ex] \sum_{k=1}^{K} \bar{N}_{R_{k,i}}, & A_{RC_{k,i}} = A_R \quad (26b) \\[1ex] 0, & \text{otherwise.} \quad (26c) \end{cases}$$

Here, the mean received number of droplets after the quantization step for the kth droplet diameter at the ith time step ($\bar{N}_{R_{k,i}}$) is defined as

$$\bar{N}_{R_{k,i}} = \begin{cases} \left\lfloor \dfrac{v_{c_{k,i}} A_{RC_{k,i}} \Delta t}{\eta r_{k,i}^3} \sum_{m=0}^{i} N_{k,i-m} + \dfrac{1}{2} \right\rfloor, & A_{RC_{k,i}} < A_R \\[3ex] & \qquad\qquad (27a) \\[1ex] \left\lfloor \dfrac{v_{c_{k,i}} A_R \Delta t}{\eta r_{k,i}^3} \sum_{m=0}^{i} N_{k,i-m} + \dfrac{1}{2} \right\rfloor, & A_{RC_{k,i}} = A_R, \\[3ex] & \qquad\qquad (27b) \end{cases}$$

where $\lfloor . \rfloor$ shows the floor function which maps a variable to the integer less than or equal to this variable. The addition with $\frac{1}{2}$ within the floor function in (27a)-(27b) provides the quantization by rounding the number of received droplets to the nearest integer.

Subsequent to quantization, the infection state of the human needs to be determined as the output of the system as shown by Figs. 1 and 4. Therefore, the detection is essential according to a threshold value (γ) as the last step of the reception. Physically, γ corresponds to the quantity of pathogen-laden droplets that suffice to make a human infected. Furthermore, γ depends on the immune system of a human. Thus, detection via the threshold γ enables to quantify the strength of the human immune system and to handle the determination of the infection state as a detection problem. Hence, the infection state (or the received symbol) can be expressed by binary hypothesis testing which is given as

$$N_{R_i} \underset{H_0}{\overset{H_1}{\gtrless}} \gamma, \qquad (28)$$

where the hypotheses H_0 and H_1 are defined as the situations of no infection as the received symbol 0 and infection

$$A_{RC_{k,i}} = r_R^2 cos^{-1}\left(\frac{d_{RC_{k,i}}^2 + r_R^2 - r_{k,i}^2}{2 d_{RC_{k,i}} r_R} \right) + r_{k,i}^2 cos^{-1}\left(\frac{d_{RC_{k,i}}^2 + r_{k,i}^2 - r_R^2}{2 d_{RC_{k,i}} r_{k,i}} \right)$$
$$- \frac{1}{2}\sqrt{\left(-d_{RC_{k,i}} + r_R + r_{k,i}\right)\left(d_{RC_{k,i}} + r_R - r_{k,i}\right)\left(d_{RC_{k,i}} - r_R + r_{k,i}\right)\left(d_{RC_{k,i}} + r_R - r_{k,i}\right)} \qquad (23)$$

Algorithm 1 Algorithm of the End-to-End System Model
___

1: **Input:** K, t_s, Δt, v_{c_0}, I_0, F_0, ρ_a, ρ_d, ρ_f, μ_a, α_e, g, $d_{(1,...,K)}$, $N_{(1,...,K),0}$, θ_0, β_{bb}, β_{ss}, initial positions of the TX and RX,

2: $t = 0 : \Delta t : t_s$

3: **for** $k = 1 : 1 : K$ **do**

4:      **for** $i = 1 : 1 : \text{length}(t)$ **do**

5:         ▷ **Step 1: Trajectory**

6:          Calculate $s_{k,i}$ by the real positive root of (6)

7:          $r_{k,i} = \alpha_e s_{k,i}$

8:          Calculate $\theta_{k,i}$ by (16)

9:          $\Delta s = s_{k,i} - s_{k,i-1}$

10:        $\Delta x = \Delta s \cos(\theta_{k,i})$; $\Delta y = \Delta s \sin(\theta_{k,i})$

11:        $x_{k,i} = x_{k,i-1} + \Delta x$; $y_{k,i} = y_{k,i-1} + \Delta y$

12:        ▷ **Step 2: Number of Droplets in the Cloud**

13:         $v_{c_{k,i}} = \Delta s / \Delta t$

14:         $Re_{k,i} = d_{k,i} v_{c_{k,i}} \rho_a / \mu_a$

15:         Calculate $v_{s_{k,i}}$ according to $Re_{k,i}$ by (22a)-(22c)

16:         Calculate $\Delta\lambda$ by (20)

17:         $\lambda_{k,i} = \lambda_{k,i-1} + \Delta\lambda$

18:         Generate $N_{k,i} \sim \mathcal{N}(\lambda_{k,i}, \lambda_{k,i})$

19:        ▷ **Step 3: Reception**

20:         **if** $(x_R - r_{k,i}) < x_{k,i} < (x_R + r_{k,i}))$ **then**

21:           $r_{CS_{k,i}} = \sqrt{r_{k,i}^2 - (x_R - x_{k,i})^2}$;

22:           $A_{CS_{k,i}} = \pi r_{CS_{k,i}}^2$

23:           Calculate $d_{RC_{k,i}}$ by (24)

24:           **if** $(r_{CS_{k,i}} - r_R) < d_{RC_{k,i}} < (r_{CS_{k,i}} + r_R)$ **then**

25:             Calculate $\bar{N}_{R_{k,i}}$ by (27a)

26:           **else if** $d_{RC_{k,i}} < (r_{CS_{k,i}} - r_R)$ **then**

27:             Calculate $\bar{N}_{R_{k,i}}$ by (27b)

28:           **else**

29:             $\bar{N}_{R_{k,i}} = 0$

30:           **end if**

31:           $N_{k,i} = N_{k,i} - \bar{N}_{R_{k,i}}$

32:         **end if**

33:      **end for**

34: **end for**

35: Calculate N_{R_i} by (26a)-(26c)

36: Determine the infection state (**h**) by applying (28)
___

as the received symbol 1, respectively. Here, the received symbol sequence with M samples is represented as $\mathbf{h} = [h_0, h_1, \ldots, h_M]$ which also gives the end-to-end system response.

D. Algorithm of the End-to-End System Model

In this part, the way to obtain the output of the end-to-end system model by employing the derivations made up to here is clarified in the proposed Algorithm 1. In the algorithm, the propagation, changing number of droplets in the cloud and their interaction with the RX are handled separately at each time step for each droplet size d_k. As the first step of the algorithm, the trajectory of the spherical cloud is calculated for each time step, i.e., the distance on the s-axis and θ values for $t = t_i$ are calculated by (6) and (16). Then, the updated

position of the cloud on the s-axis is utilized to find its step length (Δs). As shown in Fig. 2, Δs can be employed to express the step lengths on x (Δx) and y axes (Δy) as given by

$$\Delta x = \Delta s \cos(\theta_{k,i}), \Delta y = \Delta s \sin(\theta_{k,i}), \qquad (29)$$

where Δx and Δy values are used to update the cloud position on the corresponding axis. Since there is not any acting force on z-axis, the center of the cloud maintains its position on this axis. However, the cloud expands on x, y and z axes linearly due to the relation $r_{k,i} = \alpha_e s_{k,i}$ as given in Section II-A.

In the second step of Algorithm 1, the mean number of droplets in the propagating cloud is calculated. To this end, the cloud velocity ($v_{c_{k,i}}$) at the corresponding time step is calculated by the displacement on s-axis. Then, settling velocity ($v_{s_{k,i}}$) is determined by (22a)-(22c) according to $Re_{k,i}$ which is calculated by using $v_{c_{k,i}}$ and droplet size. $v_{s_{k,i}}$ is exploited to calculate the change in the mean number of droplets ($\Delta\lambda$) and thus, the mean number of droplets is updated according to this change. Here, the flow type of the cloud found by employing the velocity of droplets affects the number of droplets in the cloud.

The third step of Algorithm 1 describes the reception via the interaction of the cloud with the RX. When the cloud comes to a sufficient distance to interact with the RX, the radius of the cloud's circular cross-section ($r_{CS_{k,i}}$) is determined by the geometrical relation with the radius of the cloud and the positions of the TX and RX on the x-axis as given by

$$r_{CS_{k,i}} = \sqrt{r_{k,i}^2 - (x_R - x_{k,i})^2}, \qquad (30)$$

which allows us to calculate the circular area of the cloud's cross-section ($A_{CS_{k,i}}$). During the reception, the case that $A_{CS_{k,i}} \leq A_R$ can also be represented in terms of radii of the circles and the distance between them such that $(r_{CS_{k,i}} - r_R) < d_{RC_{k,i}} < (r_{CS_{k,i}} + r_R)$. In addition, the case for the cloud encompassing the RX ($A_{CS_{k,i}} > A_R = A_{RC_{k,i}}$) can be expressed as $d_{RC_{k,i}} < (r_{CS_{k,i}} - r_R)$. Using these conditions, the mean number of droplets given in (26a)-(26c) is calculated. Then, the detection is made according to the threshold γ in order to determine the infection state. Next, the probability of infection is derived by using the end-to-end system model.

III. PROBABILITY OF INFECTION

The probabilistic approach which is considered in the system model enables the derivation of the probability of infection of a human exposed to a sneeze or cough. To this end, it is essential to derive the probability density function (pdf) of the received number of droplets before the detection. As given in Section II-B, the number of droplets in the cloud is a Gaussian random variable for the droplet diameter of d_k and i^{th} time step, i.e., $N_{k,i} \sim \mathcal{N}(\lambda_{k,i}, \lambda_{k,i})$. Hence, its pdf ($f_N(N_{k,i})$) is given by

$$f_N(N_{k,i}) = \frac{1}{\sqrt{2\pi\lambda_{k,i}}} e^{-\frac{(N_{k,i} - \lambda_{k,i})^2}{2\lambda_{k,i}}}. \qquad (31)$$

Since the received number of droplets before the detection (N_{R_i}) is a function of $N_{k,i}$ as given in (26a)-(27b), its mean
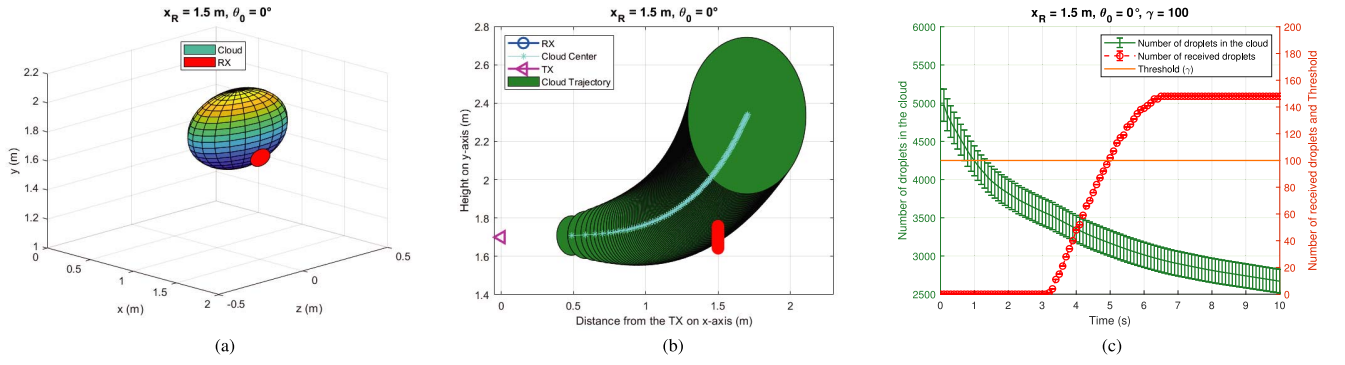
Fig. 6. The trajectory of the cloud and its interaction with the RX in (a) 3-D. (b) 2-D. (c) The number of droplets.

and variance for the reception cases can be given as

$$
E(N_{R_i}) = \begin{cases} \mu_1 = \sum_{k=1}^{K} \left\lfloor \sum_{m=0}^{i} a_{k,i}\lambda_{k,i-m} + \frac{1}{2} \right\rfloor, & A_{RC_{k,i}} < A_R \\ & (32a) \\ \mu_2 = \sum_{k=1}^{K} \left\lfloor \sum_{m=0}^{i} b_{k,i}\lambda_{k,i-m} + \frac{1}{2} \right\rfloor, & A_{RC_{k,i}} = A_R \\ & (32b) \end{cases}
$$

$$
Var(N_{R_i}) = \begin{cases} \sigma_1^2 = \sum_{k=1}^{K} \left\lfloor \sum_{m=0}^{i} a_{k,i}^2\lambda_{k,i-m} + \frac{1}{2} \right\rfloor, & A_{RC_{k,i}} < A_R \\ & (33a) \\ \sigma_2^2 = \sum_{k=1}^{K} \left\lfloor \sum_{m=0}^{i} b_{k,i}^2\lambda_{k,i-m} + \frac{1}{2} \right\rfloor, & A_{RC_{k,i}} = A_R, \\ & (33b) \end{cases}
$$

where $a_{k,i} = \frac{v_{c_{k,i}} A_{RC_{k,i}} \Delta t}{\eta r_{k,i}^3}$, $b_{k,i} = \frac{v_{c_{k,i}} A_R \Delta t}{\eta r_{k,i}^3}$, $E(.)$ and $Var(.)$ are expectation and variance operators, respectively. By using (32a)-(33b), the pdf of N_{R_i} ($f_{N_R}(N_{R_i})$) can be written as

$$
f_{N_R}(N_{R_i}) = \begin{cases} \dfrac{\exp\left(-\dfrac{(N_{R_i}-\mu_1)^2}{2\sigma_1^2}\right)}{\sqrt{2\pi\sigma_1^2}}, & A_{RC_{k,i}} < A_R \quad (34a) \\[3ex] \dfrac{\exp\left(-\dfrac{(N_{R_i}-\mu_2)^2}{2\sigma_2^2}\right)}{\sqrt{2\pi\sigma_2^2}}, & A_{RC_{k,i}} = A_R \quad (34b) \\[2ex] 0, & \text{otherwise}, \quad (34c) \end{cases}
$$

where μ_1, μ_2, σ_1^2 and σ_2^2 are defined in (32a)-(33b). The probability of infection corresponds to the situation where $N_{R_i} > \gamma$ as given by

$$
P(N_{R_i} > \gamma) = \int_{\gamma}^{\infty} f_{N_R}(u)\,du. \quad (35)
$$

The solution for (35) can be derived for the pdf given in (34a)-(34c) in terms of Q-function ($Q(x) = \frac{1}{\sqrt{2\pi}} \int_x^{\infty} \exp(\frac{-u^2}{2})du$) as given by

$$
P(N_{R_i} > \gamma) = \begin{cases} Q\left(\dfrac{\gamma - \mu_1}{\sigma_1}\right), & A_{RC_{k,i}} < A_R \quad (36a) \\[2ex] Q\left(\dfrac{\gamma - \mu_2}{\sigma_2}\right), & A_{RC_{k,i}} = A_R \quad (36b) \\[1ex] 0, & \text{otherwise}. \quad (36c) \end{cases}
$$

The derived probability of infection and the system model given in the previous section can be employed to analyze

TABLE I
EXPERIMENTAL PARAMETERS

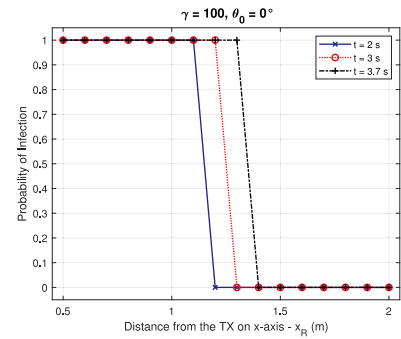| Parameter	Value	Parameter	Value
Δt	0.1 s	t_s	10 s
TX's position	(0,1.7,0) m (x,y,z)	$v_{c_{(1,\dots K),0}}$	11.2 m/s (cough) [37]
RX's position	(1.7,0) m (y,z)	g	9.81 m/s^2
I_0	0.0131 kg m/s [14]	α_e	0.2116 [40]
F_0	0.0023 kg m/s^2 [14]	β_{bb} (female)	8.853 cm [35]
ρ_d	993 kg/m^3 [38]	β_{bb} (male)	9.131 cm [35]
ρ_f (at $34°C$)	0.98 kg/m^3 [39]	β_{ss} (female)	6.901 cm [35]
ρ_a (at $23°C$)	1.172 kg/m^3 [14]	β_{ss} (male)	7.57 cm [35]
μ_a	19×10^{-6} kg/(m s) [14]		

Fig. 7. Probability of infection according to distance for different time values.

the dynamics of the pathogen transmission as given with the numerical results in the next section.

IV. NUMERICAL RESULTS

In this section, numerical results using the algorithmic end-to-end system model and derived probability of infection are given. The values of the experimental parameters are given in Table I which includes values obtained by empirical studies [14], [35], [37]–[40]. Furthermore, the initial number of droplets according to their diameters for a cough is given in Table II. For sneezing, there are not sufficient empirical data in the literature to obtain the parameter values given in Table I such as α_e and initial velocity [15]. Therefore, although our proposed model is applicable to a sneezing scenario, we only consider a coughing scenario for two static humans where one of them is the TX and the other is RX. For the results in Figs. 6–7, the dimensions of the RX are applied by using the average values of male and female humans. Namely, β_{bb} and β_{ss} are obtained by calculating the average of the female and male values given in Table I.
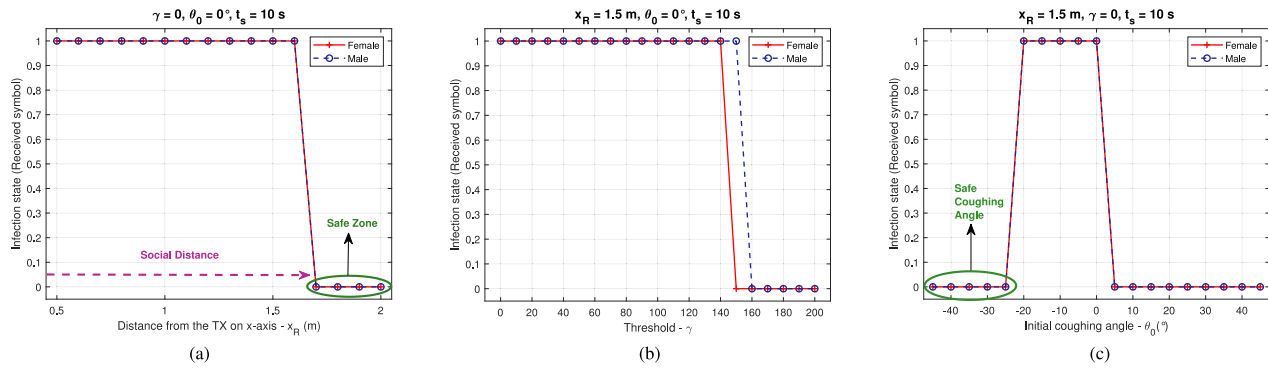
Fig. 8. Infection state of the RX with respect to (a) x_R, (b) γ, and (c) θ_0.

TABLE II
INITIAL NUMBER OF DROPLETS [26]

d (μm)	Quantity (cough)	d (μm)	Quantity (cough)	d (μm)	Quantity (cough)
2	50	40	240	200	35
4	290	50	110	250	29
8	970	75	140	500	34
16	1600	100	85	1000	12
24	870	125	48	2000	2
32	420	150	38	Total	4973

For $x_R = 1.5$ m and $\theta_0 = 0°$, Figs. 6 (a) and (b) depict the trajectories of the cloud with respect to RX in 3-D and 2-D, respectively. Due to initial momentum of coughing and net buoyant force, the cloud propagates in the horizontal and vertical directions, respectively. As also observed in these trajectories, the 3-D cloud can encompass (or intersect with) the RX and the RX is exposed to droplets during the passage of the cloud. Fig. 6 (c) shows the interaction of a human who can be infected with a disease-spreading human by quantifying the number of droplets received from the cloud. The number of droplets are given by their mean and their variations (vertical bars) due to the Gaussian distribution. These variations are calculated as three times the standard deviation (99.73% confidence interval) for each sample. The standard deviation for the received number of droplets is not observed in Fig. 6 (c), since it is relatively small with respect to the mean value. As observed in Fig. 6 (c), the number of droplets in cloud decreases, since large-sized droplets settle due to the gravity. As mentioned in Section II, the RX gets infected, when the received number of droplets is above γ as plotted in Fig. 6 (c). This figure shows the importance of the exposure time which is the interval of the changing zone in the received signal. If the RX is exposed to the cloud less, it is possible not to be infected, since the received number of droplets can be below γ. This interaction is also clarified in Fig. 7 by showing the relation of the infection probability with the distance for different propagation time instances. Actually, this figure reveals that if the RX is exposed to the cloud for a longer period, the RX is more likely to be infected.

Different scenarios can be analyzed by employing the infection state, which is the output of the end-to-end system model, for various x_R, γ, θ_0 values and male/female receivers. In Fig. 8 (a), γ is set to zero to determine the safe zone where there is no possibility of infection. This safe zone starts at $x_R = 1.7$ m which also shows the minimum social distance. Fig. 8 (c) shows

that initial coughing angle affects the infection state severely. For θ_0 values between 0 and -25 degrees, it is more likely to infect someone due to the buoyant forces. Therefore, it is safer to cough with an initial angle $\theta_0 \leq -25°$ which is depicted as safe coughing angle in Fig. 8 (c). Coughing with $\theta_0 \geq 0°$ may not be safe, since aerosols can suspend in the air and settle eventually due to gravity or drift due to indoor air currents in the long term. In Figs. 8 (a) and (c), the results are indistinguishable for male and female receivers. However, Fig. 8 (b) shows that the infection states of female and male humans can be affected differently for the same γ values due to the slight difference in the face dimensions.

In this paper, numerical results are based on our model which focuses on the propagation and reception of droplets in the outer layer of the human face. For a more rigorous model, the effect of turbulent flows and the survival rate of pathogens can be taken into account. The reception part can be improved by considering the interaction of pathogens with the human cells. In addition, γ can be estimated by considering several effects such as age, chronic diseases and genetic factors. These improvements are left as open research issues.

V. CONCLUSION

In this paper, an algorithmic end-to-end system model is proposed for droplet-based communication via coughing/sneezing between two static humans. The TX emits a cloud which is a mixture of droplets and air and it propagates under the influence of the initial momentum, gravity and buoyancy. A receiver model which defines the central part of the human face as the RX cross-section is proposed to give an output of infection state of the RX. The transmitted and received number of droplets are modeled as random processes which lead us to derive the probability of infection. It is revealed that the initial coughing angle of the TX and the detection threshold which actually corresponds to the strength of the human immune system are significant parameters to model the airborne pathogen transmission. As the future work, we plan to extend our study for mobile TXs and RXs.

APPENDIX

For a settling droplet, the downwards net force for a spherical droplet at the ith time step with the diameter d_k is

given as

$$F_{down_i} = G_i - B_i = V_d\rho_d g - V_d\rho_a g$$
$$= \frac{\pi d_{k,i}^3}{6}(\rho_d - \rho_a)g. \tag{37}$$

Furthermore, an upward drag force acts in the opposite direction of gravity due to the interaction of the droplet with the air. This upward drag force is given as [27]

$$F_{up_i} = \frac{1}{2}\rho_d v_s^2 \pi \frac{d_{k,i}^2}{4} C_D, \tag{38}$$

where C_D is the drag coefficient. For the settling condition, these upward and downward forces are in equilibrium. Hence, we can obtain the settling velocity by equating these two forces and pulling out v_s as given by

$$v_{s_{k,i}} = \sqrt{\frac{4d_{k,i}g(\rho_d - \rho_a)}{3\rho_d C_D}}. \tag{39}$$

Here, C_D changes according to Re as given by [32]

$$C_D = \begin{cases} \dfrac{24}{Re}, & Re < 2 \text{ (Stokes flow)} & (40a) \\ \dfrac{18.5}{Re^{3/5}}, & 2 \le Re \le 500 \text{ (Intermediate flow)} & (40b) \\ 0.44, & 500 < Re \le 2 \times 10^5 \text{ (Newton's flow)}. \\ & & (40c) \end{cases}$$

When the drag coefficients in (40a)-(40c) and Re in (21) are substituted into (39), the settling velocities in (22a)-(22c) can be obtained.

REFERENCES

[1] B. Atakan, *Molecular Communications and Nanonetworks: From Nature to Practical Systems*. New York, NY, USA: Springer, 2014.

[2] H. Unterweger *et al.*, "Experimental molecular communication testbed based on magnetic nanoparticles in duct flow," in *Proc. Int. Workshop Signal Process. Adv. Wireless Commun.*, 2018, pp. 1–5.

[3] F. Gulec and B. Atakan, "A droplet-based signal reconstruction approach to channel modeling in molecular communication," *IEEE Trans. Mol. Biol. Multi-Scale Commun.*, vol. 7, no. 1, pp. 64–68, Mar. 2021.

[4] S. Bhattacharjee *et al.*, "A testbed and simulation framework for air-based molecular communication using fluorescein," in *Proc. 7th ACM Int. Conf. Nanoscale Comput. Commun.*, 2020, pp. 1–6.

[5] M. Abbaszadeh *et al.*, "Mutual information and noise distributions of molecular signals using laser induced fluorescence," in *Proc. IEEE Global Commun. Conf.*, 2019, pp. 1–6.

[6] L. Khaloopour *et al.*, "An experimental platform for macro-scale fluidic medium molecular communication," *IEEE Trans. Mol. Biol. Multi-Scale Commun.*, vol. 5, no. 3, pp. 163–175, Dec. 2019.

[7] M. Hamidović, U. Marta, G. Fink, R. Wille, A. Springer, and W. Haselmayr, "Information encoding in droplet-based microfluidic systems: First practical study," in *Proc. ACM Int. Conf. Nanoscale Comput. Commun.*, 2019, pp. 1–6.

[8] F. Gulec and B. Atakan, "Distance estimation methods for a practical macroscale molecular communication system," *Nano Commun. Netw.*, 2020, Art. no. 100300, May 2020.

[9] F. Gulec and B. Atakan, "Fluid dynamics-based distance estimation algorithm for macroscale molecular communication," *Nano Commun. Netw.*, vol. 28, Jun. 2021, Art. no. 100351.

[10] S. Qiu *et al.*, "Long range and long duration underwater localization using molecular messaging," *IEEE Trans. Mol. Biol. Multi-Scale Commun.*, vol. 1, no. 4, pp. 363–370, Dec. 2015.

[11] F. Gulec and B. Atakan, "Localization of a passive molecular transmitter with a sensor network," in *Proc. Int. Conf. Bio-Inspired Inf. Commun.*, 2020, pp. 317–335.

[12] M. Khalid, O. Amin, S. Ahmed, B. Shihada, and M.-S. Alouini, "Communication through breath: Aerosol transmission," *IEEE Commun. Mag.*, vol. 57, no. 2, pp. 33–39, Feb. 2019.

[13] M. Khalid, O. Amin, S. Ahmed, B. Shihada, and M.-S. Alouini, "Modeling of viral aerosol transmission and detection," *IEEE Trans. Commun.*, vol. 68, no. 8, pp. 4859–4873, Aug. 2020.

[14] L. Bourouiba, E. Dehandschoewercker, and J. W. Bush, "Violent expiratory events: On coughing and sneezing," *J. Fluid Mech.*, vol. 745, pp. 537–563, Apr. 2014.

[15] Z. Ai and A. K. Melikov, "Airborne spread of expiratory droplet nuclei between the occupants of indoor environments: A review," *Indoor Air*, vol. 28, no. 4, pp. 500–524, 2018.

[16] B. Killingley and J. Nguyen-Van-Tam, "Routes of influenza transmission," *Influenza Respir. Viruses*, vol. 7, no. 2, pp. 42–51, 2013.

[17] R. Mittal, R. Ni, and J.-H. Seo, "The flow physics of covid-19," *J. Fluid Mech.*, vol. 894, pp. F2-1–F2-14, Jul. 2020.

[18] J. Wei and Y. Li, "Human cough as a two-stage jet and its role in particle transport," *PloS One*, vol. 12, no. 1, 2017, Art. no. e0169235.

[19] J. Wei and Y. Li, "Enhanced spread of expiratory droplets by turbulence in a cough jet," *Build. Environ.*, vol. 93, pp. 86–96, Nov. 2015.

[20] X. Xie, Y. Li, A. T. Y. Chwang, P. L. Ho, and W. H. Seto, "How far droplets can move in indoor environments-revisiting the wells evaporation-falling curve," *Indoor Air*, vol. 17, no. 3, pp. 211–225, 2007.

[21] B. Wang, H. Wu, and X.-F. Wan, "Transport and fate of human expiratory droplets—A modeling approach," *Phys. Fluids*, vol. 32, no. 8, 2020, Art. no. 083307.

[22] M.-R. Pendar and J. C. Páscoa, "Numerical modeling of the distribution of virus carrying saliva droplets during sneeze and cough," *Phys. Fluids*, vol. 32, no. 8, 2020, Art. no. 083305.

[23] T. Dbouk and D. Drikakis, "On coughing and airborne droplet transmission to humans," *Phys. Fluids*, vol. 32, no. 5, 2020, Art. no. 053310.

[24] G. Busco, S. R. Yang, J. Seo, and Y. A. Hassan, "Sneezing and asymptomatic virus transmission," *Phys. Fluids*, vol. 32, no. 7, 2020, Art. no. 073309.

[25] V. Vuorinen *et al.*, "Modelling aerosol transport and virus exposure with numerical simulations in relation to SARS-COV-2 transmission by inhalation indoors," *Safety Sci.*, vol. 130, Oct. 2020, Art. no. 104866.

[26] J. Duguid, "The size and the duration of air-carriage of respiratory droplets and droplet-nuclei," *Epidemiol. Infect.*, vol. 44, no. 6, pp. 471–479, 1946.

[27] B. R. Munson, D. F. Young, T. H. Okiishi, and W. W. Huebsch, *Fundamentals of Fluid Mechanics*. Hoboken, NJ, USA: Wiley, 2009.

[28] B. R. Morton, G. I. Taylor, and J. S. Turner, "Turbulent gravitational convection from maintained and instantaneous sources," *Proc. Royal Soc. A, Math. Phys. Eng. Sci.*, vol. 234, no. 1196, pp. 1–23, 1956.

[29] N. De Cock, M. Massinon, S. O. T. Salah, and F. Lebeau, "Investigation on optimal spray properties for ground based agricultural applications using deposition and retention models," *Biosyst. Eng.*, vol. 162, pp. 99–111, Oct. 2017.

[30] R. A. Shaw, "Particle-turbulence interactions in atmospheric clouds," *Annu. Rev. Fluid Mech.*, vol. 35, no. 1, pp. 183–227, 2003.

[31] A. Papoulis and S. U. Pillai, *Probability, Random Variables, and Stochastic Processes*. New York, NY, USA: Tata McGraw-Hill Educ., 2002.

[32] M. Reuter *et al.*, *The Metrics of Material and Metal Ecology: Harmonizing the Resource, Technology and Environmental Cycles*. London, U.K: Elsevier, 2005.

[33] J. S. Peiris, K. Y. Yuen, A. D. M. E. Osterhaus, and K. Stöhr, "The severe acute respiratory syndrome," *New England J. Med.*, vol. 349, no. 25, pp. 2431–2441, 2003.

[34] B. Atakan and F. Gulec, "Signal reconstruction in diffusion-based molecular communication," *Trans. Emerg. Telecommun. Technol.*, vol. 30, no. 12, 2019, Art. no. e3699.

[35] J. W. Young, "Head and face anthropometry of adult U.S civilians," Office Aviation Med, Federal Aviation Admin., Washington, DC, USA, Rep. DoT/FAA/AM-93/10, 1993.

[36] E. W. Weisstein. (2003). *Circle-Circle Intersection*. Accessed: Jun. 15, 2020. [Online]. Available: https://mathworld.wolfram.com/Circle-CircleIntersection.html

[37] S. Zhu, S. Kato, and J.-H. Yang, "Study on transport characteristics of saliva droplets produced by coughing in a calm indoor environment," *Build. Environ.*, vol. 41, no. 12, pp. 1691–1702, 2006.

[38] M. Nicas, W. W. Nazaroff, and A. Hubbard, "Toward understanding the risk of secondary airborne infection: Emission of respirable pathogens," *J. Occup. Environ. Hyg.*, vol. 2, no. 3, pp. 143–154, 2005.

[39] A. Picard, R. Davis, M. Gläser, and K. Fujii, "Revised formula for the density of moist air," *Metrologia*, vol. 45, no. 2, p. 149, 2008.

[40] J. W. Tang, T. J. Liebner, B. A. Craven, and G. S. Settles, "A schlieren optical study of the human cough with and without wearing masks for aerosol infection control," *J. Royal. Soc. Interface*, vol. 6, no. 6, pp. S727–S736, 2009.